Solid Oxide Electrolysis Cells: Microstructure and Degradation of the Ni/Yttria-Stabilized Zirconia Electrode

Hauch, Anne; Ebbesen, Sune; Jensen, Søren Højgaard; Mogensen, Mogens Bjerg

Published in:
Journal of the Electrochemical Society

Link to article, DOI:
10.1149/1.2967331

Publication date:
2008

Document Version
Publisher's PDF, also known as Version of record

Journal of The Electrochemical Society, **155** (11) B1184-B1193 (2008)
0013-4651/2008/155(11)/B1184/10/$23.00 © The Electrochemical Society

Solid Oxide Electrolysis Cells: Microstructure and Degradation of the Ni/Yttria-Stabilized Zirconia Electrode

A. Hauch,[z] S. D. Ebbesen, S. H. Jensen,[*] and M. Mogensen[*]

Fuel Cells and Solid State Chemistry Department, Risø DTU, National Laboratory for Sustainable Energy, Technical University of Denmark, DK-4000 Roskilde, Denmark

Solid oxide fuel cells produced at Risø DTU have been tested as solid oxide electrolysis cells for steam electrolysis by applying an external voltage. Varying the sealing on the hydrogen electrode side of the setup verifies that the previously reported passivation over the first few hundred hours of electrolysis testing was an effect of the applied glass sealing. Degradation of the cells during long-term galvanostatic electrolysis testing [850°C, −1/2 A/cm^2, $p(H_2O)/p(H_2)$ = 0.5/0.5] was analyzed by impedance spectroscopy and the degradation was found mainly to be caused by increasing polarization resistance associated with the hydrogen electrode. A cell voltage degradation of 2%/1000 h was obtained. Postmortem analysis of cells tested at these conditions showed that the electrode microstructure could withstand at least 1300 h of electrolysis testing, however, impurities were found in the hydrogen electrode of tested solid oxide electrolysis cells. Electrolysis testing at high current density, high temperature, and a high partial pressure of steam [−2 A/cm^2, 950°C, $p(H_2O)$ = 0.9 atm] was observed to lead to significant microstructural changes at the hydrogen electrode-electrolyte interface.
 [DOI: 10.1149/1.2967331]

Manuscript submitted March 31, 2008; revised manuscript received July 11, 2008. Published September 22, 2008.

Considering the increasing interest in renewable energy, the hydrogen economy and CO_2 neutral energy production, the reversible solid oxide cell (SOC) is a potential technology for electricity production [solid oxide fuel cells (SOFCs)], as well as for hydrogen and synthetic fuel production [solid oxide electrolysis cells (SOECs)].[1]

Already in the 1980s researchers in the HotElly project[2-4] and at Westinghouse[5] published promising results on hydrogen production by steam electrolysis using SOECs and electricity-to-hydrogen efficiency above 90% was reported.[4] During the 1990s and 2000s the research and development (R&D) focus has been on the R&D for SOFCs rather than SOECs, and material development and optimization has led to large improvements in performance and durability for SOFCs and decreased production cost for SOFCs. The necessity to store energy from the increasing amounts of electricity from renewable energy sources has renewed the interest for using SOCs for electrolysis purposes, and recently several research groups have reported on SOEC R&D work.[6-16]

From a fundamental thermodynamic and electrochemical point of view it is clear that high temperature electrolysis of steam can provide H_2 with high efficiency and high purity, and SOECs can be used as buffers to optimize the efficiency of intermittent sources, such as wind power, and utilize waste heat and surplus energy from, e.g., nuclear power facilities during off-peak hours. However, for these cells to become successful from a technological and commercial point of view for H_2 and synthetic fuel production, SOECs need to be cost competitive, high performing, and long-term stable. Even though promising electrolysis results have been obtained for SOECs, economic estimates for potential H_2 and CH_4 production price using SOECs also indicate that considerable improvements of the SOECs, especially the long-term stability, is necessary to make these cells competitive to existing H_2 and synthetic fuel production methods.[1,17,18]

Previously we have reported on the high initial electrolysis performance for SOCs produced at Risø DTU and shown that a significant passivation[a] occurs for the SOECs over the first few hundred hours of operation. However, the cells can be partly reactivated either by fuel cell operation of the cell or continued galvanostatic electrolysis operation at constant conditions.[12] Postmortem analyses of tested SOECs showed that significant amounts of impurities had segregated to the hydrogen electrode/electrolyte interface of heavily passivated SOECs. It was proposed that at least a part of these impurities originated from the applied albite glass sealing used in the setup for cell testing.[19] However, electrolysis test data to support the hypothesis of the effect of the glass sealing on the passivation of the SOECs was not presented, neither did the work include investigation of microstructural changes of the electrodes upon testing and possible relation to observed loss in performance of the SOCs.

In this article we present results on long-term galvanostatic steam electrolysis test of SOCs applying different sealing materials, and long-term degradation results that do not originate from glass sealing effects are provided. Microstructures of the hydrogen electrode of long-term tested SOECs are related to the hydrogen electrode structures of reference cells, to the loss in performance for the SOECs and to similar long-term tested SOFCs. Microstructure of the hydrogen electrode of an SOEC tested at high current density (−2 A/cm^2) is presented and data that show that impurities in the hydrogen electrode of tested SOECs cannot only originate from the glass sealing.

Experimental

Ni/yttria-stabilized zirconia (YSZ) SOCs were used for the electrolysis tests. The cells were full cells produced at Risø DTU.[20,21] The cells had a 10–15 μm thick hydrogen electrode of Ni/YSZ cermet and were supported by a ~300 μm thick Ni/YSZ layer, a 10–15 μm thick YSZ electrolyte, and a 15–20 μm thick LSM-YSZ composite oxygen electrode.[20] The ratio between Ni (Alfa Aesar, Johnson Matthey Company) and YSZ (TZ8Y, Tosoh Corporation, ZrO_2 stabilized with 8 mol % Y_2O_3) was 40/60 vol % both for the support layer and the active electrode layer.[22] ZrO_2 stabilized with 3 mol % Y_2O_3 was used for the support layer. The composition of the LSM was $(La_{0.75}Sr_{0.25})_{0.95}MnO_3$ and the ratio between LSM and YSZ in the composite electrode was LSM/YSZ = 50/50 vol %.[23] Analyses of the exact chemical composition of the raw materials were checked by glow discharge mass spectroscopy (GDMS) and listed elsewhere.[19] From the GDMS analyses the maximum quantities of the impurities present in the raw materials and relevant for the postmortem analysis of tested cells presented were: 13 ± 1 ppm Si, 8 ± 1 ppm Al, and up to 680 ± 40 ppm Na.

The SOCs were planar 5 × 5 cm cells with an active electrode area of 16 cm^2. The setup for cell testing, i.e., alumina housing, current collector (Ni foil), glass sealing, and Ni/YSZ based gas distributor is illustrated and described in detail elsewhere.[12,24,25] The top part of the alumina cell housing had a current collector (gold foil) and an air distributor (LSM based), and was placed on top of the bottom part of the alumina cell housing to give a cross flow for the gases.[12] The sealing usually applied for this cell test setup were

* Electrochemical Society Active Member.
[z] E-mail: anne.hauch@risoe.dk

[a] "Passivation" is used to describe a reversible or partly reversible loss in performance for the cell, whereas "degradation" is used to describe an irreversible loss in performance for the cell.

Table I. Test duration and conditions for the galvanostatic electrolysis tests. Oxygen was passed over the O_2 electrode for all tests. The inlet gas compositions to the H_2 electrode are given. The theoretical steam conversion was 28% for all tests.

Test number	Test duration (h)	Sealing	Test conditions
A	1316	Albite glass	850°C, $p(H_2O)/p(H_2)$ = 0.5/0.5, −0.5 A/cm^2
B	1510	Albite glass[a]	850°C, $p(H_2O)/p(H_2)$ = 0.5/0.5, −0.5 A/cm^2
C	694	Gold	850°C, $p(H_2O)/p(H_2)$ = 0.5/0.5, −0.5 A/cm^2
D	68	Albite glass	950°C, $p(H_2O)/p(H_2)$ = 0.9/0.1, −2.0 A/cm^2

[a] The albite glass sealing was pretreated for 12 days at 950°C and $p(H_2O)$ = 0.9 atm prior to reducing the NiO in the Ni/YSZ electrode and starting the electrolysis testing.

bars of albite glass ($NaAlSi_3O_8$) mixed with YSZ.[19,26] The start-up procedure, including heating ramp (1°C/min to 1000°C), reduction procedure (9% H_2 in N_2 and pure H_2), and initial characterization of the cell performance (*i-V* curves in fuel cell and electrolysis mode and electrochemical impedance spectroscopy) are described elsewhere.[12,26]

The electrolysis tests were performed galvanostatic. An overview of the long-term electrolysis test specifications and duration is given in Table I. The gas passing over the oxygen electrode was pure O_2 and the inlet gas composition to the hydrogen electrode was $p(H_2O)$ = 0.5 atm and $p(H_2)$ = 0.5 atm for tests A, B, and C, which was obtained by mixing 6 L/h O_2 and 24 L/h H_2 in a gas mixer and led to the cell through the inlet tube. By applying pure oxygen to the oxygen electrode before, upon the start of and during electrolysis testing the $p(O_2)$ was kept constant at 1 atm when switching from open circuit voltage (OCV) to electrolysis operation of the cell. To keep a constant $p(O_2)$ was advantageous for subsequent analyses of the possible changes in the oxygen electrode response observed in the electrochemical impedance spectra recorded during testing, because the $p(O_2)$ affects the electrokinetcs significantly. For the high current density test D, steam was supplied by an evaporator box (DV2MK including heat transfer line from aDROP Feuchtemessstecknik GmbH). The theoretical degree of steam conversion was calculated as the number of converted water molecules using Faraday's law, divided by the total number of H_2O molecules supplied to the gas inlet of the cell. For all the tests in Table I, the theoretical steam conversion was 28%. Besides the SOCs used for steam electrolysis testing (Table I), two cells where selected as reference cells. Reference cells were obtained by applying the usual heating up and NiO-reduction procedure to the cells from the same production batch as the cells used for electrolysis testing. After obtaining a cell voltage close to the one expected from the calculated Nernst potential, the cells were cooled down and these reference cells were used for scanning electron microscopy (SEM) investigations for comparison with tested cells.

Electrochemical impedance spectra (EIS) were recorded using a Solartron 1260 frequency analyzer. For impedance measurements during electrolysis testing, i.e., under current load, the Solartron 1260 was used in combination with an external shunt to measure the ac through the cell as described elsewhere.[26] The software Zview 2.8 was used for the analyses the impedance spectra.[27]

Pieces of the reference cells and electrolysis tested cells were subjected to field emission (FE) SEM analyses and microanalyses were obtained by energy dispersive spectroscopy (EDS). A Zeiss Supra 35 FE-SEM equipped with a Noran System SIX X-ray microanalysis system was used for these postmortem analyses. The cells were prepared for SEM investigation by vacuum embedding pieces of the cells in epoxy (EpoFix from Struers) followed by grinding and polishing. The samples were subsequently coated with carbon to eliminate charging. It has been shown that the presence of epoxy as mounting material does not interfere with the impurity analysis.[28]

Results

The initial performance of the cells was measured by *i-V* curves at various temperatures and partial pressures of steam to the Ni/YSZ electrode and by EIS. Test A had a nonoptimal Ni current collector foil which led to a large ohmic resistance (0.16 Ω cm^2) compared to standard values for this type of cells (~0.10 Ω cm^2) at 850°C.[29] The ohmic (R_s) and polarization resistances (R_p) given in Table II were obtained from EIS recorded at the beginning and end of the galvanostatic electrolysis tests at the test conditions given in Table I, i.e., under current load.

Long-term electrolysis testing, cell voltage curves.— Figure 1 shows the cell voltage for the three long-term tested SOECs, i.e., tests, A, B, and C, [850°C, −0.5 A/cm^2, $p(H_2O)/p(H_2)$ = 0.5/0.5]. The cell voltage measured at the start of test A was 1143 mV, but in Fig. 1 the cell voltage curve for test A has been subtracted an "offset" of 68 mV to ease the comparison of the cell voltage curves for the two longest tested SOECs, tests A and B.

Rods of albite glass were used as sealing material for test A.[24] The same type of albite glass sealing was used for test B, however after heating to 950°C and prior to reduction of the NiO in the Ni/YSZ electrode and start of electrolysis testing, the sealing was exposed to 950°C and $p(H_2O)$ = 0.9 atm for 12 days to evaporate

Table II. Overview of ohmic resistances (R_s) and polarization resistances (R_p) obtained from impedance spectra recorded at the beginning and end of each electrolysis test under the electrolysis test conditions given in Table I. ΔR_s and ΔR_p are calculated as: $(R_{end} - R_{start})/R_{start} \times 100$. R_s and R_p values for tests A, B, and C are results from the fit of experimental spectra. R_s and R_p values for test D are obtained directly from Nyquist plot of the recorded EIS.

Test number	Test duration (h)	$R_{s,start}$ (Ω cm^2)	$R_{s,end}$ (Ω cm^2)	ΔR_s, (%)	$R_{p,start}$ (Ω cm^2)	$R_{p,end}$ (Ω cm^2)	ΔR_p (%)
A	1316	0.14	0.16	10	0.23	0.32	36
B	1510	0.08	0.09	13	0.18	0.28	56
C	694	0.10	0.11	7	0.33[a]	0.43	32
D	68	0.15	0.45	200	0.33	0.44	21

[a] R_p for test C is dominated by a large gas conversion impedance response (summit frequency ~1 Hz) of 0.18 Ω cm^2 compared to more typical values at these operation conditions such as 0.04 Ω cm^2 for test A and 0.05 Ω cm^2 for test B.

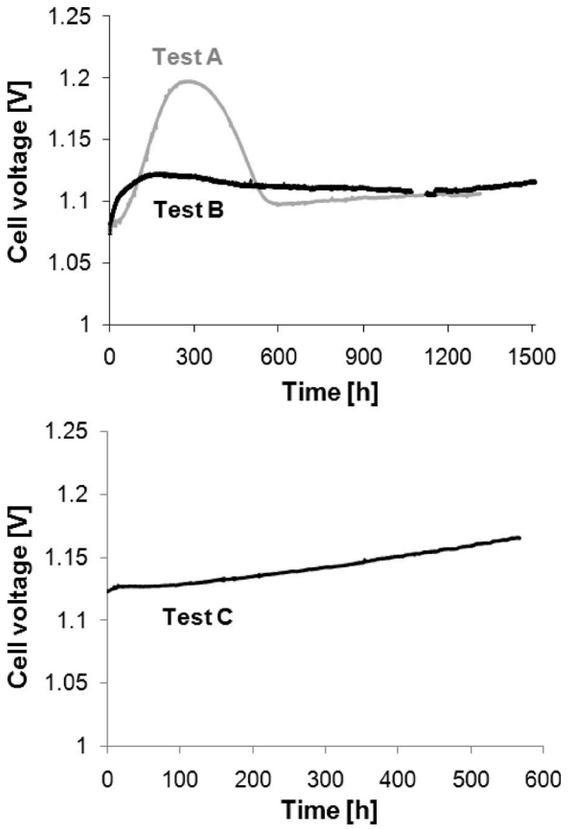

Figure 1. Cell voltage vs time for tests A, B, and C during electrolysis testing (Table I). The albite glass sealing used for test B was pretreated for 12 days at 950°C and $p(H_2O) = 0.9$ atm and $p(O_2) = 0.1$ atm. The difference in cell voltage between tests A and B at the start of electrolysis testing has been subtracted from the cell voltage curve of test A (68 mV). For test C the albite glass sealing was substituted by a coiled gold foil and platinum paste on the hydrogen electrode side of the cell test setup.

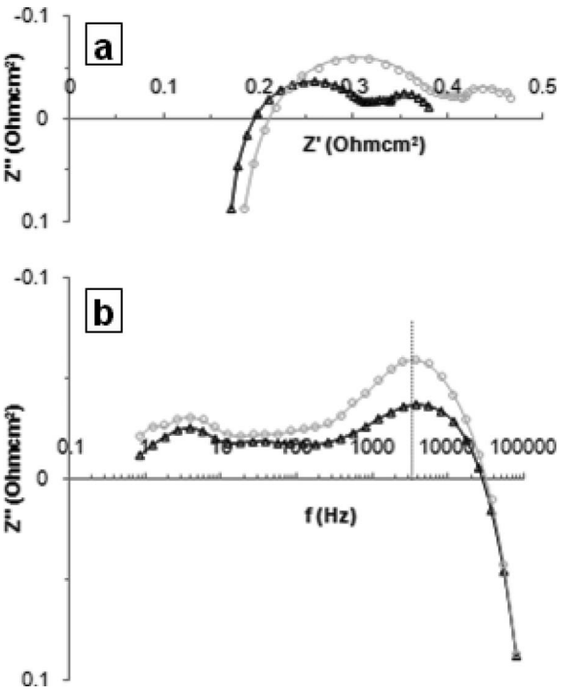

Figure 2. Impedance spectra recorded under current load (−0.5 A/cm^2) during test A after 1 h (black Δ) and 1293 h (gray O) of electrolysis testing. Spectra were recorded from 82 kHz to 0.8 Hz with 6 points per frequency decade. (a) Nyquist plot and (b) imaginary part of the Bode plot. The dashed line (~3.3 kHz) mark the frequency region at which the impedance spectrum have changed the most upon electrolysis testing.

$Si(OH)_4$ from the surface of the albite glass prior to electrolysis testing. From the cell voltage curves in Fig. 1 applying different sealing material for the hydrogen electrode part of the cell test setup it can be observed that the transient phenomenon for test A, i.e., passivation followed by activation, is closely related to the use of albite glass as sealing material. This transient phenomenon can be avoided using gold foil and Pt paste as sealing material for the hydrogen electrode part of the cell test setup as for test C. In all cases albite glass sealing was used for the oxygen electrode side of the cell test setup. From tests A and C long-term cell voltage degradation rates of 2%/1000 h for test A and 5%/1000 h for test C were obtained.

Long-term electrolysis testing, degradation measured by EIS.— The long-term degradation was monitored by recording EIS during electrolysis testing, i.e., under current load. Figure 2 shows two typical impedance spectra recorded in the beginning and end of test A. The most dominant change for the impedance spectrum recorded after 1293 h of electrolysis testing occurs in the frequency range 2–4 kHz (Fig. 2b). Applying the model by Barfod et al.[30] for the breakdown of losses in this type of hydrogen electrode supported cells, it has been possible to break down the polarization losses during electrolysis testing into five RQ-equivalent circuit contributions: (*i*) a high frequency LSM electrode arc ($R_{LSM,h}$) with a summit frequency in the range 10^4–10^5 Hz, (*ii*) a Ni electrode arc (R_{Ni}) with a summit frequency in the range 2×10^3–10^4 Hz, (*iii*) a low frequency LSM electrode arc ($R_{LSM,l}$) with a summit frequency in the range 100–2×10^3 Hz, (*iv*) a gas diffusion arc (R_{diff}) with a summit frequency in the range 10–100 Hz, and (*v*) a gas conversion arc (R_{conv}) with a summit frequency in the range 1–10 Hz. R_{diff} and R_{conv} also originate from the Ni/YSZ electrode.

Figure 3 shows the development of R_s and the three contributions describing the resistance to the electrochemical reactions at the two electrodes, i.e., $R_{LSM,h}$, R_{Ni} and $R_{LSM,l}$, during the long-term degradation for tests A and C. The measurement at which the relative error between experimental and fitted value for the EIS was at a maximum was below 8% for all analyzed spectra. EIS from the beginning and end of test B has been used as a measure of the long-term degradation for test B. The breakdown of losses for these two EIS for test B showed the same trend as for test A.

From Fig. 3 it is evident that the resistance due to the charge transfer at the Ni-YSZ interface[31] i.e., R_{Ni}, accounts for the main part of the loss in performance for the SOECs during the long-term degradation for both tests A and C. R_{diff} and R_{conv} are not shown as they do not describe electrochemical reactions at the electrodes. The increase in R_{Ni} is linear in time for both tests A and C in accordance with the linear increase in cell voltage observed for the long-term degradation (Fig. 1). Table III summarizes the increases in the different electrode contributions to R_p and R_s for tests A, B, and C. The changes in R_s, $R_{LSM,h}$, R_{Ni} and $R_{LSM,l}$ given in Table III are obtained from optimal fit of experimental impedance spectra in the beginning and end of electrolysis tests A, B, and C. The changes in R_{diff} are 0.005 Ω cm^2/1000 h for all three tests. The increase in R_{conv} is 0.01 Ω cm^2/1000 h for tests A and B, but significantly higher for test C (0.08 Ω cm^2/1000 h). Analysis of the EIS recorded during the short term passivation related to the use of albite glass sealing for test A is dealt with in detail elsewhere.[32]

Microstructure of the long-term tested SOECs.— Figure 4 shows examples of FE-SEM images of a cross section of a reference

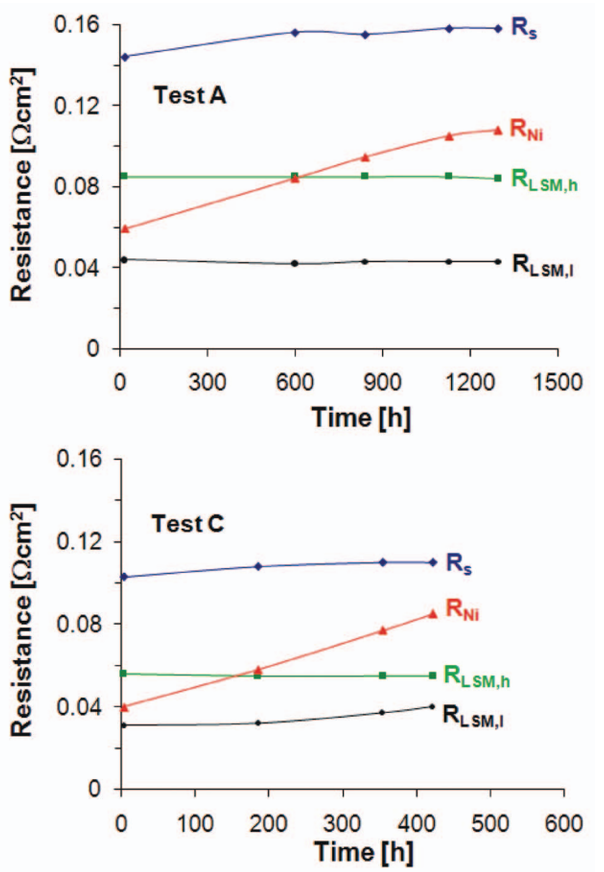

Figure 3. Development of R_s, $R_{LSM,h}$, R_{Ni}, and $R_{LSM,l}$, during long-term electrolysis tests A and C. The equivalent circuit model by Barfod et al. (Ref. 30) and the software Zview was applied (Ref. 27) to obtain optimal fit of the experimental EIS.

cell and the cell used for test A. Cell pieces from tests B and C show similar microstructures to the ones shown in Fig. 4 and cross section FE-SEM images of test B are given elsewhere.[33]

Comparing the overview images of the reference cell (Fig. 4a) and the cell used for test A (Fig. 4d) it is evident that the 1300 h of electrolysis testing (test A) has not caused obvious micron scale structural changes and there are no macroscopic cracks in the electrolyte. The higher magnification images of the oxygen electrode/electrolyte interface of the reference cell (Fig. 4b) and the cell used for test A (Fig. 4e) show that the composite LSM-YSZ electrode structure is preserved for the tested cell both regarding particle sizes and porosity. There is still an unchanged proper contact between the electrode and the electrolyte even after 1300 h of electrolysis testing. The higher magnification images of the hydrogen electrode/electrolyte interface of the reference cell (Fig. 4c) and the cell used for test A (Fig. 4f) show that no large damages to the Ni/YSZ electrode structure has occurred. The Ni particles are nonoxidized, have an acceptable particle size and the porosity of the active electrode is preserved.

In Fig. 4c and f the Ni particles appear to be on top of the YSZ in the electrode due to the sharp gray scale variations at the Ni and YSZ particle phase boundary. However, this is not a topographic effect but an effect of the differences in interaction volumes in the two phases as described by Bilde-Sørensen who used the hydrogen electrode from test B for illustration of this effect.[34]

Microstructure vs loss in performance for long-term tested SOECs.— Due to the results from EIS during electrolysis testing a more detailed quantitative analysis of possible microstructural changes of the Ni/YSZ electrode was performed, i.e., Ni particle size distributions for the active electrode layer of reference and tested cells was determined. The method for obtaining Ni particle size distributions was adapted from the work by Hagen et al.[21] The size distributions of Ni particles were therefore obtained by superimposing a set of parallel lines with a pitch of 1 μm on the innermost 10 μm of the Ni/YSZ electrode closest to the electrolytes. The chord lengths within Ni particles were measured. The uncertainty for the measured chord lengths is estimated to be ±0.05 μm for the micrographs used for the Ni particle size distributions given here. The distribution of chord lengths was then used as a measure of Ni particle size distributions.

An overview of the key parameters (mean Ni chord length, number of Ni particles/300 μm line, Ni coverage and number of Ni particles included in the size distribution) for the Ni particle size distributions for reference cells, cells from tests A, B, and C, a heavily passivated SOEC,[19] and for an SOC used for long-term fuel cell testing[21] is given in Table IV. From the numbers in Table IV it is evident that the Ni particle size distribution has changed upon testing both for electrolysis and fuel cell tested SOCs. Within the uncertainty, the mean Ni chord lengths are identical for the four electrolysis tested cells and the fuel cell tested cell. Further, key test parameters and total loss in performance for each of the tests are given Table IV. It is observed that change in area specific resistance (ΔASR) for the five tested cells presented in Table IV varies from 12 to 332%.

Impurities in the Ni/YSZ electrode of long-term tested SOECs.— Several pieces (~1 cm long each) of the electrolysis tested cells have been investigated by FE-SEM and EDS in the search for impurities. Using these analytical tools no impurities have been found in the oxygen electrode of the electrolysis tested cells or in any part of the reference cells. Based on the electrolysis test results at least three different cases should be studied in detail in relation to impurities in the Ni/YSZ electrode. That is cell pieces from tests where case (*i*) a normal glass sealing was used and no reactivation of the cell was obtained during electrolysis testing, i.e., the test was stopped at the maximum loss in performance, case (*ii*) a normal glass sealing was used but the cell was allowed to reactivate after it had reached the maximum loss in performance (test A), and case (*iii*) a gold sealing was used to minimize impurities originating from the cell test setup (test C).

For case 1 FE-SEM and EDS results were reported previously and showed significant quantities, up to ~8 wt % SiO_2, of Si-containing impurities in the few micrometers of the Ni/YSZ elec-

Table III. Overview of the changes in R_s, $R_{LSM,h}$, R_{Ni}, and $R_{LSM,l}$ obtained from optimal fit of experimental impedance spectra in the beginning and end of electrolysis tests A, B, and C. The changes in resistances have been normalized to 1000 h. Changes in resistances that are below 0.005 Ω cm² per 1000 h are within the uncertainty and reported as zero.

Test number	ΔR_s/1000 h (Ω cm²)	$\Delta R_{LSM,h}$/1000 h (Ω cm²)	ΔR_{Ni}/1000 h (Ω cm²)	$\Delta R_{LSM,l}$/1000 h (Ω cm²)
A	0.01	0	0.04	0
B	0.01	0	0.05	0.02
C	0.02	0	0.10	0

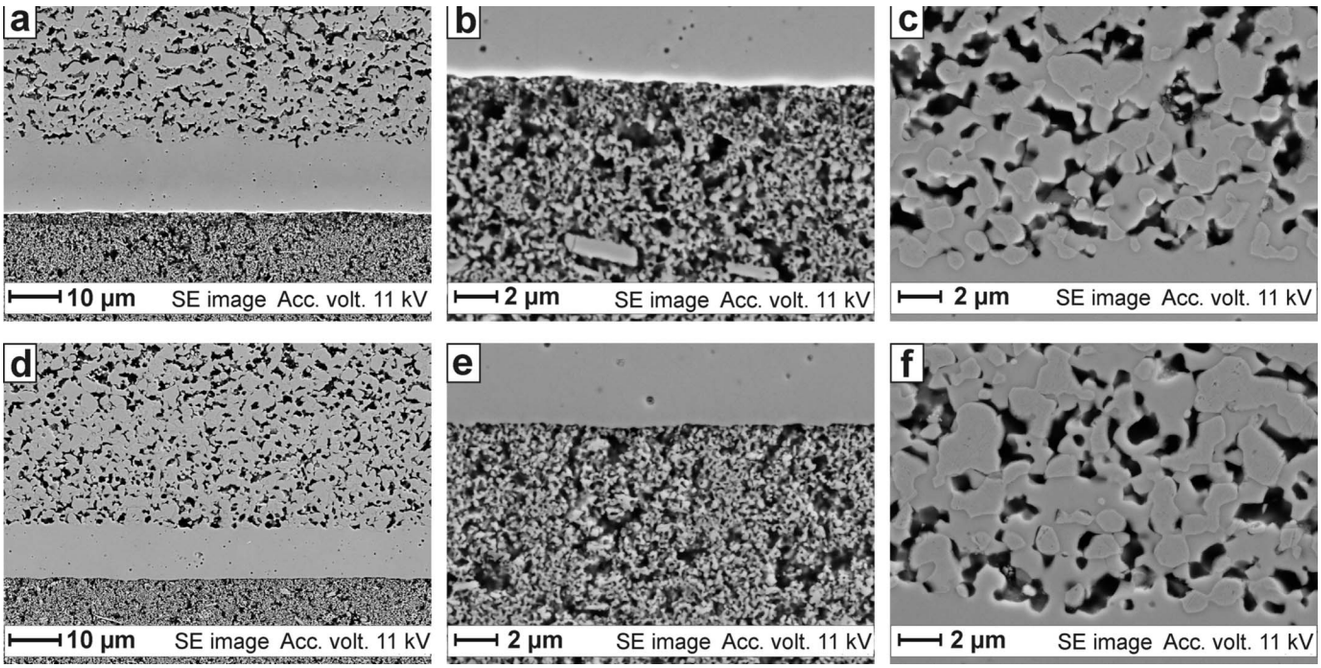

Figure 4. (a) Overview SEM image of a cross section of a reference cell. The hydrogen electrode is at the top part, the electrolyte in the middle and the oxygen electrode in the bottom of the image, (b) SEM image of the oxygen electrode of a reference cell, (c) SEM image of the hydrogen electrode of a reference cell, (d) overview SEM image of a cross section of the cell from test A, (e) SEM image of the oxygen electrode of the cell from test A, and (f) SEM image of the hydrogen electrode of the cell from test A.

trode closest to the electrolyte was found.[19] In case 2, which corresponds to test A, microanalysis of the YSZ-Ni/YSZ interface shows that Si-containing impurities can be found in this electrode. Figure 5 shows an example of Si-containing impurities in the hydrogen electrode from test A. Figure 5a shows a SEM micrograph of the electrolyte-hydrogen electrode interface from the cell used for test A and Fig. 5b shows the EDS map of the same region as Fig. 5a. Cross section of four pieces (~1 cm long each) from the cell used for test A were subjected to thorough FE-SEM and microanalysis investiga-

Table IV. Electrolysis test conditions, change in area specific resistances (ASR) and Ni particle size distributions for differently tested SOECs and SOFC. ASR values are the sum of R_s and R_p obtained from EIS at OCV, 850°C, 20% H_2O to the hydrogen electrode. The first and last EIS at these conditions for each test have been used to calculate $\Delta ASR = (ASR_{start}\text{-}ASR_{end})/ASR_{start} \times 100$. The last row gives the number of Ni particles counted for each size distribution. Numbers in brackets are for a reference cell from the same production batch as the cells for which results were reported previously (Ref. 19).

Test number	Ref.	A	B	C	Heavily passivated SOEC[a]	FC-tested SOC[b]
Test conditions	—	850°C, $p(H_2O)$ = 0.5 atm, $-\frac{1}{2}$ A/cm^2	850°C, $p(H_2O)$ = 0.5 atm, $-\frac{1}{2}$ A/cm^2	850°C, $p(H_2O)$ = 0.5 atm, $-\frac{1}{2}$ A/cm^2	850°C, $p(H_2O)$ = 0.7 atm, -1 and $-\frac{1}{2}$ A/cm^2	850°C, $CO_2/H_2 = \frac{1}{4}$, -1.9 A/cm^2
Duration (h)	—	1316	1510	694	580	1500
ΔASR (%)	—	15	24	146[b]	332	12
Mean Ni chord lengths (µm)	1.01 ± 0.05[c] (1.04 ± 0.05)	1.26 ± 0.05	1.22 ± 0.05	1.24 ± 0.05	1.24 ± 0.05	1.22 ± 0.04
Number of Ni particles/300 µm line	84 (86)	63	66	66	66	—
Ni coverage (%)	28 (29)	26	27	27	27	—
No. of Ni particles	509 (542)	512	536	588	336	~300

[a] Ref. 19.
[b] Hagen et al. (Ref. 21 showed the histogram for the Ni particle size distribution, however, the number behind the given histogram as they appear here were kindly provided by co-author Dr. Yi-Lin Liu who also determined the mean Ni intercept length for a reference cell to be 1.04 ± 0.04 µm.
[c] The total loss in performance (ΔASR) for test C was increased further by 8 h of steam starvation caused by a failure in the steam supply. The degradation rate before and after this failure in the steam supply was indentical, however an abrupt increase in the cell voltage was observed due to this steam starvation.

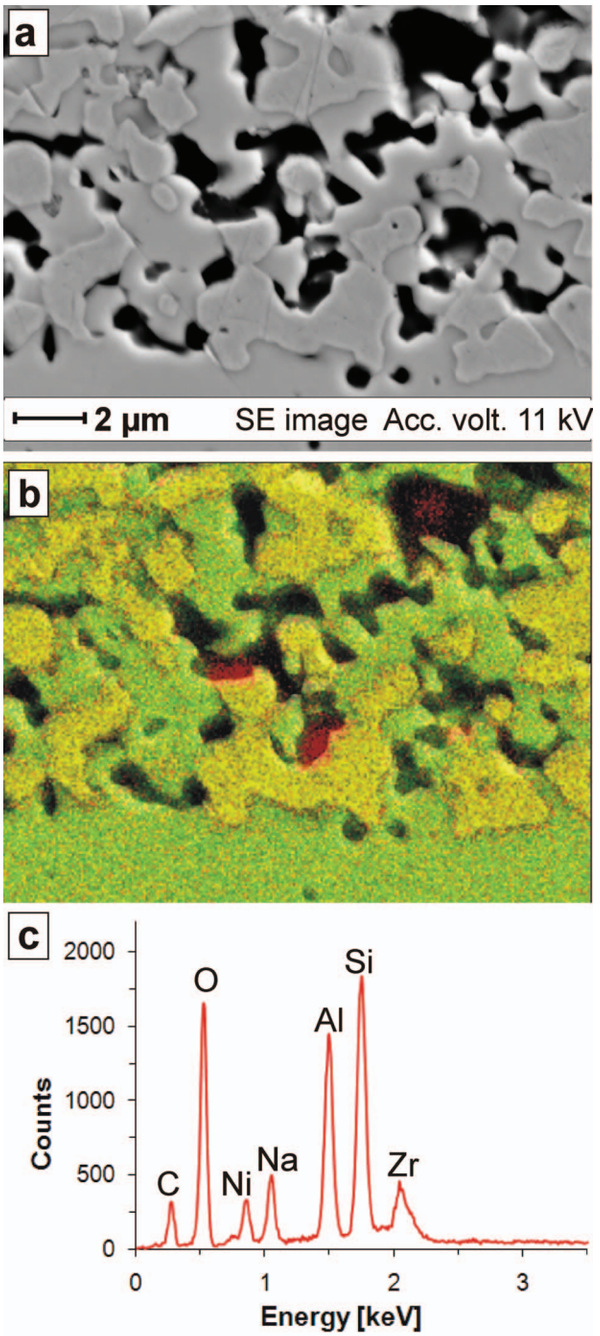

Figure 5. (a) SEM micrograph of the hydrogen electrode from the cell used for test A. (b) EDS map of the same region as a). Zr is green, Ni is yellow, and Si is red. For clarity the element maps for Al and Na have not been overlaid. (c) EDS (point analysis) of the Na and Al containing silicate impurity closest to the electrolyte in (b).

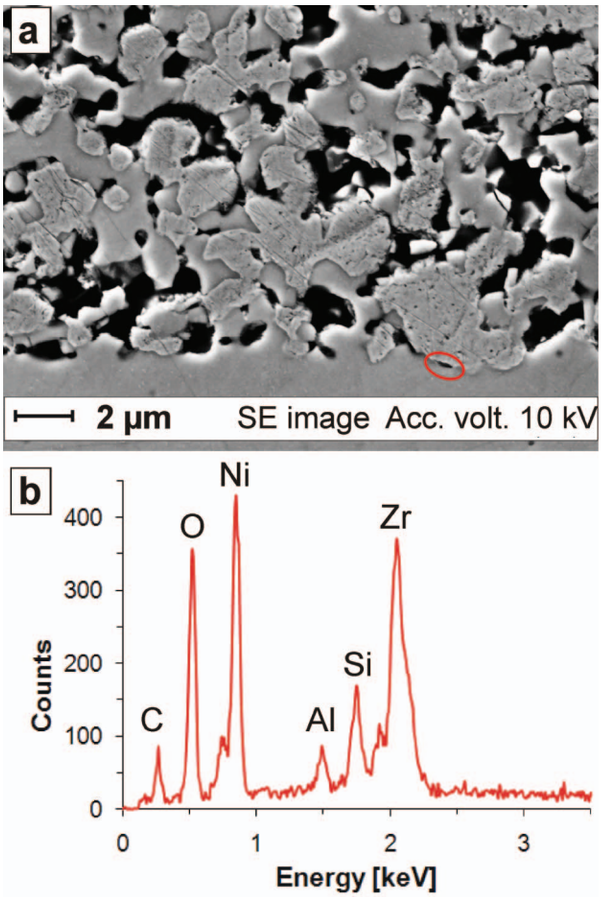

Figure 6. (a) SEM micrograph of the hydrogen electrode from the cell used for test C applying a gold foil and Pt paste as sealing. (b) EDS (point analysis) of the Si-containing impurity marked by the circle in (a).

tions. Only limited quantities of impurities were detected in the Ni/YSZ electrode and nowhere could impurities in the quantities as those reported for case 1 be found (column six in Table IV).[19] The impurities shown in Fig. 5 represent a maximum both regarding the size of the accumulated impurities and the quantity of impurities in a certain area of the Ni/YSZ electrode of the cell used for test A. Figure 5c shows the point EDS result obtained for the impurity phase closest to the electrolyte in Fig. 5b. This and the other impurity particles in this part of the cell piece from test A are sodium and aluminum containing silicates.

In case 3, which is the case for test C, the quantities of impurities found in the Ni/YSZ electrode are significantly lower than in the case 2 (test A). However, even though a gold sealing and platinum paste was used as sealing material for test C, impurities could be detected in the active layer of the Ni/YSZ electrode by EDS in a bulk SEM sample. Figure 6 shows an example of a Si-containing impurity phase in the cell used for test C.

Microstructural changes of the Ni/YSZ electrode for the high current density test D.— Five pieces (each ~1 cm long) of the cell used for the high current density test D was investigated by FE-SEM and EDS. Si-containing impurities were found in some regions of the cell pieces. All impurities were located within the innermost 10 µm of the hydrogen electrode closest to the electrolyte and the quantity of impurities appear to be less than the extreme case as reported previously,[19] but more than that illustrated for test A (Fig. 5). Figure 7 shows that significant microstructural changes have occurred at the electrolyte-hydrogen electrode interface in some regions of the cell operated at high current density (test D). From Fig. 7 it is observed that a dense Ni-YSZ layer of a thickness of approximately 2–4 µm has formed. Here Ni appears to have relocated and filled the porosity of the first few microns of the Ni/YSZ electrode closest to the YSZ electrolyte. The scratches in the Ni particles in the SEM micrograph (Fig. 7) originate from nonoptimal polishing of the sample.

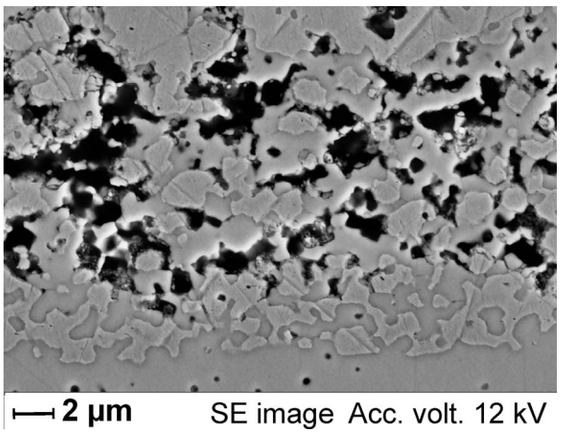

Figure 7. SEM micrograph of the electrolyte-hydrogen electrode interface from the cell used for the "high current density" test D.

Discussion

Long-term electrolysis testing, effect of cell test setup.— Comparison of cell voltage curves for the long-term electrolysis tests A, B, and C, where the only difference was variations in the sealing material used for the hydrogen electrode part of the cell test setup, clearly show that the choice of the sealing material influences the development of the cell voltage during galvanostatic electrolysis testing. It is well known that a high partial pressure of steam at high temperatures leads to a considerable partial pressure of $Si(OH)_4$ over different silicates.[35,36] A $p(Si(OH)_4)$ of $\sim 1 \times 10^{-7}$ atm can be expected over an albite glass at the temperature and gas composition as for test D (Table I).[19] As described and analyzed in detail by Jensen.[32] the initial passivation of cell in test A is caused by a shift in the equilibrium from gaseous $Si(OH)_4$ toward formation of glassy phase silicates at the triple-phase-boundaries (3PB) in the Ni/YSZ electrode upon steam reduction that is started when the electrolysis current load is applied. The activation of the cell can be due to crystallization and reorganization of the Si-containing impurities in the hydrogen electrode. The effect of the pretreatment of glass sealing, as it was done for test B, supports the hypothesis that the evaporation of $Si(OH)_4$ from the glass sealing is a main factor in the initial passivation for these SOECs. However, the cell voltage curve for test B (Fig. 1) does not provide a clear picture of evaporation of Si species from the applied glass sealing on the passivation, activation, and subsequent and underlying long-term degradation for these SOECs.

The cell voltage curve for test C, using gold and Pt paste as sealing material, is free of the passivation/activation phenomenon and thereby provides the evidence that the passivation over the first few hundreds of electrolysis tests reported previously[12] and the passivation/activation phenomenon observed for test A is an effect of the use of albite glass sealing on the hydrogen electrode part of the cell test setup. Other groups are using glass as a sealing material for SOEC testing and have reported significant loss in performance.[37] They stated that a "stable performance was demonstrated" for their single cell test, but the cell voltage and development of cell resistance during electrolysis testing for 300 h revealed an increase in cell resistance from 0.5 to 0.62 Ω cm^2, which corresponds to an increase in cell voltage of $\sim$20% per 1000 h at 800°C and -0.7 A/cm^2. However, data and analyses to describe whether this loss in performance, or part of it was related to use of glass sealing were not provided. Development of alternative and inexpensive sealing materials or development of proper coatings for glass sealing is a necessity for SOECs. From a technological, and especially commercial, point of view, the use of expensive gold sealing as for test C is not feasible. However, from a scientific point of view the use of gold sealing can significantly contribute to the understanding of the processes involved in the long-term degradation of the SOECs.

Long-term electrolysis testing, long-term degradation.— For the long-term electrolysis tests A and B the increase in R_s values are comparable to the R_s increase reported by Hagen et al.[21] for similar cells tested in fuel cell mode.

Recording EIS for gas variation experiments at OCV prior to and after electrolysis testing for test A has indicated that the long-term degradation occurs at the Ni/YSZ electrode of the SOEC.[26] This is confirmed by the fit and breakdown of losses for the EIS recorded during electrolysis testing (Fig. 3). In general, it can be concluded from the analysis of EIS during electrolysis test A, B, and C (Table III) that it is the increase in the Ni/YSZ electrode response that, by far, dominates the increase in R_p during long-term electrolysis testing. This is not the case for long-term fuel cell testing of similar cells.[21] R_{Ni} was reported to be caused by resistance to charge transfer at the Ni-YSZ.[31]

Primdahl and Mogensen[38] analyzed the impedance caused by the gas conversion in the Ni/YSZ electrode and found summit frequencies of $\sim$1–5 Hz and expressed the gas conversion resistance, R_{conv}, obtained from EIS as

$$R_{conv} = \frac{RT}{4F^2 J_i}\left(\frac{1}{x_{i,H_2O}} + \frac{1}{x_{i,H_2}}\right) \quad [1]$$

where R is the gas constant, F is Faraday's constant, T is the temperature, J_i is the inlet area specific flow rate (mol/m^{2}s), x_{i,H_2O} and x_{i,H_2} are the inlet mole fractions of steam and hydrogen, and it is assumed that $\Delta x_{i,H_2O} \ll x_{i,H_2O}$ and $\Delta x_{i,H_2O} \ll x_{i,H_2}$ during the perturbations caused by the impedance measurements. For test C the arc caused by gas conversion was large ($R_{conv} = 0.18\ \Omega\ cm^2$) compared to the gas conversion arcs for tests A and B ($\sim 0.05\ \Omega\ cm^2$). Based on pO_2 inlet measurements it can be assumed that the molar fractions of H_2O and H_2 to the inlet of the cells have been identical for the electrolysis tests, and the actual inlet flow to the Ni/YSZ electrode of test C has been significantly lower than the feed of 12 L/h H_2O and 12 L/h H_2 given by the flow meters.

This in turn leads to a higher steam utilization for test C compared to tests A and B. An *i-V* curve recorded at 850°C and applying 12 L/h H_2O and 12 L/h H_2 showed a tendency for steam starvation already at a current density of $-\frac{1}{2}$ A/cm^2 corresponding to conversion of approximately 3.6 L/h H_2O using Faraday's law. *i-V* curves at these conditions for tests A, and B, and other similar cells,[12] do not show the effect of steam starvation even at the double current density. Further, R_{conv} increased 0.08 Ω cm^2/1000 h for test C but only 0.01 Ω cm^2/1000 h for tests A and B.

Considering the observed high steam utilization with tendency for steam starvation, test C can be expected to suffer from uneven current distribution compared to the current distributions for tests A and B. Even though test C was also operated at a total current of 8 A as tests A and B, there has most likely been relatively large differences in the "local" current density between different regions of the 4×4 cm cell for test C. Such uneven current distribution in the Ni/YSZ will, in turn, lead to a larger ΔR_{Ni} compared to SOECs operated with an optimal current distribution, and this is the case when comparing ΔR_{Ni} for tests A, B, and C.

In summary, the analyses of EIS during long-term electrolysis testing show that solving the short term passivation, i.e., the glass sealing dependent passivation, observed for test A and reported previously for similar SOECs,[12] is only part of the problem related to the hydrogen electrode part of the SOECs. The long-term degradation is also mainly due to loss in performance of the Ni/YSZ electrode. The long-term SOEC degradation rates are higher than SOFC degradation rates and improved long-term stability is a necessity from a commercial/economical point of view.

Microstructure of the SOC electrodes.— Generally the microstructure of the tested electrolysis cells have sustained hundreds of hours of testing at what can be considered moderate electrolysis test conditions (850°C, -0.5 A/cm^2, 50% H_2O) without significant changes. There is no tendency for delamination between the electrolyte and the O_2 electrode, even though such problems with delamination of the O_2 electrode from the electrolyte has been reported and has been suggested to be caused by pressure differences occurring upon O_2 evolution in closed pores in the electrode/electrolyte interface.[17,39-41] Such delamination must be considered a question of optimizing processing techniques to preserve an optimal contact between the electrolyte and the LSM based electrode upon electrolysis testing. From a technological point of view it is important to notice that inexpensive production methods such as spraying and screen printing can be applied and still provide LSM based O_2 electrodes with microstructures able to sustain thousands of hours as O_2 evolution electrodes with no delamination from the electrolyte (Fig. 4e).

SEM work on the hydrogen electrode of tested SOECs (Fig. 4e) clearly provides evidence that an inexpensive production method, such as tape casting, can be used for producing SOEC hydrogen electrodes that can withstand thousand of hours of electrolysis testing, simultaneously maintaining a satisfactory contact to the electrolyte, porosity, and no oxidation of the Ni particles.

To the best of our knowledge no other detailed SEM work has been presented on electrodes from long-term tested state-of-the-art SOECs. In the 1980s Dönitz and co-workers[4] reported on long-term stability of electrolyte supported tubular SOECs using Ni/YSZ hydrogen electrodes. However, a comparison of the effect of long-term electrolysis testing on the microstructure of Ni/YSZ electrodes by Dönitz and co-workers[4] and the results presented in Fig. 4 cannot be given for two reasons: (*i*) the Ni/YSZ microstructure presented by Dönitz et al.[4] was from a starting point significantly more coarse than the Ni/YSZ structures presented here and (*ii*) satisfactory SEM work on the electrode structure after long-term testing was not provided by Dönitz et al.[4]

Microstructure vs loss in performance.— The procedure for obtaining the Ni particle size distributions was adapted from Hagen et al.[21] but it can be questioned whether or not a different method for obtaining the Ni particle size distributions could lead to different characteristic numbers for the Ni particle size distributions. However, the Ni particle size distributions given in Table IV are all obtained in the same manner and for cells that are identical from a production point of view. This justifies a comparison of the Ni size distributions for reference cells, differently tested SOECs and the fuel cell tested cell. For the Ni particle size distributions presented here a layer of 10 μm from the electrolyte was investigated as this constitutes the active electrode layer from a production point of view. Further, Brown et al.[42] found a thickness of the electrochemically active layer of ~10 μm for Ni/YSZ cermet electrodes at 1000°C. The thickness of the electrochemically active layer varies with temperature and microstructure of the electrode. The microstructures of the electrodes used by Brown et al.[42] were coarser than those of the SOECs tested here and the thickness of the electrochemically active layer for the tested SOECs is presumably 5–10 μm.

Even though the cells have been exposed to different test conditions and suffer from extremely different degrees of degradation, it is evident from the characteristic numbers for the Ni particle size distributions (Table IV) that the tested SOECs (columns 3–6, Table IV) have similar Ni particle size distributions. Therefore the changes in the Ni size distributions from a reference cell to an electrolysis tested cell cannot be the main factor for the observed degradation of the tested SOECs.

Comparing the Ni size distributions for tests A and B with the somewhat shorter test C, it is evident that the coarsening of the Ni particles occurs before 700 hours of testing at 850°C and a $p(H_2O)$ of 0.5 atm. From studies of Ni catalysts it is well known that a high $p(H_2O)/p(H_2)$ lead to coarsening of Ni particles and it has been reported that a high $p(H_2O)$ at OCV lead to a rapid (less than 100 h) change in the Ni size distribution.[43,44] Even though the changes of the Ni particle size distribution is more rapid at a high $p(H_2O)$, it does not increase the overall coarsening of the Ni particles. The Ni particle size distributions for electrolysis tested cells where a $p(H_2O)$ of 0.98–0.99 atm has been applied for 300–450 h are identical to the Ni particle size distributions given for the tested cells in Table IV.[26]

Further, there is a striking similarity between the Ni particle size distributions for long-term electrolysis tested cell and the fuel cell tested cell with a low degradation rate reported by Hagen et al.[21] This again shows that the larger degradation rates of these SOCs when tested as electrolysis cells compared to fuel cell testing is not an effect of changes in the Ni particle size distributions.

Impurities in the Ni/YSZ electrode.— Applying gold instead of albite glass as a sealing material on the hydrogen electrode side of the setup clearly minimized the quantities of impurities found in the hydrogen electrode closest to the electrolyte. The FE-SEM and EDS results for test C (Fig. 6) show that additional Si-containing impurities, which do not originate from the glass sealing on hydrogen electrode side of the cell test setup, are observed in electrolysis tested cells.

It is well known that impurities such as Si, Na, and Al from the bulk of YSZ can segregate to the grain boundaries, external surfaces, and interfaces when annealed at 800–1500°C,[45] and previously Si-containing impurities have been found in half-cells in a setup with YSZ electrolyte pellets,[28,46,47] where it was believed that the Si-containing impurities segregated from the Ni electrode and the YSZ electrolyte to the electrode/electrolyte interface. Therefore, another very likely source for the impurities found in the cell from test C is the raw materials; however other "external" impurity sources cannot be excluded. The fact that no Si was detected using FE-SEM/EDS in two reference cells verifies that the accumulation of impurities at the hydrogen electrode/electrolyte interface, to the extent observed for the tested cells, is a result of the electrolysis testing of the cells and not merely a result of the production method of the cells.

From the FE-SEM/EDS analysis of the cell used for test A (Fig. 5) it seems plausible that the impurity phases are located at what is presumed to be 3PB in the Ni/YSZ electrode prior to degradation. A transmission electron microscope (TEM) study of the Ni/YSZ electrode from test A supports the findings in Fig. 5. In this TEM study six impurities in the TEM lamellae were all located at boundaries between a Ni particle, a YSZ particle and a pore.[48] Combining the cell test results for test A (Fig. 1 and 3) with the postmortem results for the Ni/YSZ electrode of this cell (Fig. 5) two different mechanisms, or a combination of them, can explain the impurity findings in the cell from test A: (*i*) The activation of the SOEC is not caused by evaporation of the Si species from the 3PB, but rather a redistribution or crystallization of the impurities, which lead to a fewer number of blocked 3PB or (*ii*) the impurities found in the hydrogen electrode of test A are caused by the long-term degradation, where impurities from the raw materials could accumulate at the 3PB. Considering the large differences in the shape of the impurities found in the cell from test A (round shaped particles, up to ~1 μm in diameter) with those found previously for a nonreactivated cell (40–70 nm thick rims between Ni and YSZ particles), it seems plausible that the reactivation of test A can be obtained by changes in the physical properties and redistribution of the impurity phases and not necessarily by a decrease in the total amount of impurities present in the hydrogen electrode.

High current density test D.— Estimates of hydrogen production prices using SOECs have shown that for SOEC systems lasting a couple of years, a current density of -1.5 A/cm^2 and higher will most likely be necessary for SOECs to become a price competitive option for large scale hydrogen production.[1] In this context the high current density test D is interesting even though it can hardly be considered a long-term electrolysis test.

The loss in performance for test D is significantly different in size and nature from tests A, B, and C, as the increase in the resistance for test D is completely dominated by the 200% increase in the R_s (Table II) within only 68 h of electrolysis testing. Qualitatively the extensive and probably irreversible microstructural changes of the YSZ-Ni/YSZ interface observed for the cell used for test D (Fig. 7) correspond well to the very large increase in the R_s during testing.

Figure 8 shows a sketch to illustrate a possible mechanism for the changes in the microstructure at the YSZ-Ni/YSZ interface observed for the high current density test D (Fig. 7). At high temperatures and high $p(H_2O)$; e.g., 950°C and at $p(H_2O) = 0.9$ atm and $p(H_2) = 0.1$ atm as for test D; a relatively high partial pressure of nickel hydroxide, $Ni(OH)_2$, of approximately 1×10^{-8} atm can be expected[b] as indicated in Fig. 8a. Oxygen ions will be conducted in the YSZ toward the oxygen electrode when the external voltage is applied and steam electrolysis started (Fig. 8b). Ni particles will be equipotentials, but there will be an electrical resistance in the YSZ particles of the Ni/YSZ electrode and an electrical potential gradient outwards in the YSZ as indicated by $\uparrow\Delta\varphi$ in Fig. 8b. The 3PB closest to the electrolyte (marked by red squares in Fig. 8b) will be more strongly reducing (high current density) than the blue marked 3PB (lower current density) and the Ni(II) in the mobile nickel hydroxide will most likely be reduced to metallic Ni at the strongly reducing points. An overall reaction scheme is

$$Ni(OH)_2(g) + 4e^- \rightarrow Ni(s) + 2O^{2-} + H_2(g) \qquad [2]$$

Such relocation of Ni will consequently lead to a dense Ni-YSZ layer as observed in the SEM image in Fig. 7. Other parts of the cell may contain Ni(II) species, however it will be the large potential difference near the electrode/electrolyte interface during electrolysis testing that is the "driving force" for the electrochemical reduction of Ni(II) to metallic Ni at this interface for test D.

Further studies of SOECs operated at current densities above -1.5 A/cm^2 are necessary to verify the proposed hypothesis for the observed microstructural changes of the YSZ-Ni/YSZ interface put forward here. Preferably, such tests should be performed free of cell test "set-up artifacts," such as the passivation effect of the glass sealing. Changes such as those observed for the YSZ-Ni/YSZ interface for the high current density test D strongly point toward that development of an alternative hydrogen electrode using different materials than Ni and YSZ is necessary if there is a demand for SOEC systems to be operated at high temperature, high $p(H_2O)$ and high current density e.g., -2 A/cm^2 and higher.

Conclusion

From the results presented here we conclude the following:

1. The initial passivation of the solid oxide electrolysis cells reported previously and observed for test A originate from Si species from the applied glass sealing and can be avoided by replacing the albite glass sealing on the hydrogen electrode side of the cell test setup and thereby avoid Si species from the sealing being deposited in the Ni/YSZ electrode.
2. The long-term degradation of SOECs, e.g., a cell voltage degradation of 2% [850°C, $-\frac{1}{2}$ A/cm^2, $p(H_2O)/p(H_2) = 0.5/0.5$] is higher than for long-term fuel cell testing of similar cells and need to be lowered.
3. Analyses of electrochemical impedance spectra recorded during electrolysis testing show that the main part of the long-term degradation (free of passivation effects from the sealing material) of the SOECs is caused by increased losses in the hydrogen electrode. However the mechanism behind the long-term degradation is not understood yet.
4. FE-SEM characterization shows that the microstructures of the tested SOECs can sustain more than 1300 h of testing at 850°C,

[b] Based on thermochemical calculations using the software FactSage.

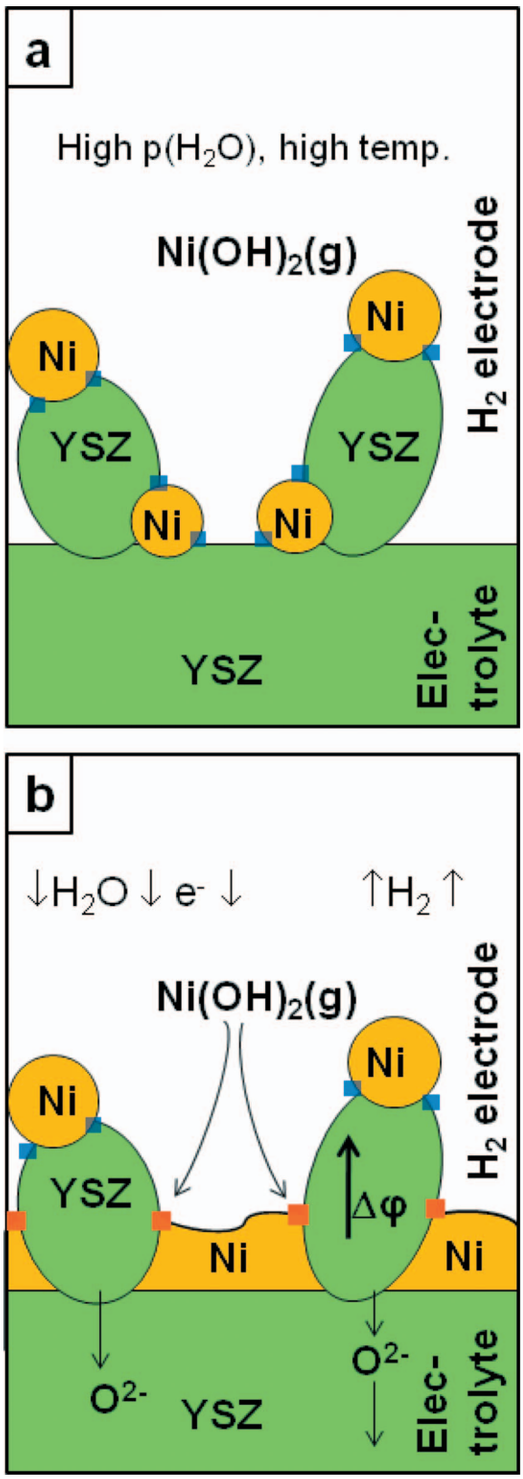

Figure 8. Illustration of the possible mechanism for the changes in the microstructure at the YSZ-Ni/YSZ interface observed for the high current density test D (Fig. 7). (a) The YSZ-Ni/YSZ interface at OCV prior to degradation at high current density electrolysis testing. 3PB are marked by blue squares. The high $p(H_2O)$ and high temperature lead to a considerable activity of $Ni(OH)_2$. (b) The YSZ-Ni/YSZ interface upon degradation at high current density electrolysis testing. There will be electrical resistance in the YSZ particles and the electrical potential gradient in the YSZ particles is illustrated by $\Delta\varphi$. The 3PB marked by red squares will be more reducing points than those 3PB marked by blue squares and the reduction of nickel hydroxide will take place at the red marked 3PB leading to a dense Ni-YSZ layer.

$-\frac{1}{2}$ A/cm^2, $p(H_2O)/p(H_2) = 0.5/0.5$. The electrodes have maintained their high porosity and no delamination from the electrolytes were observed.

5. The mean Ni particle size has changed from 1.01 ± 0.05 μm for a reference cell to $\sim 1.24 \pm 0.05$ μm for the electrolysis tested cells. However, this is not the main factor for the loss in performance for Ni/YSZ. A similar change in mean Ni particle size has been observed for similar long-term tested SOFCs for which a significantly lower degradation rate was reported.

6. Si-containing impurities have been found in the Ni/YSZ electrode of all tested SOECs, but not in the reference cells. Most of the impurities also contain Al and Na. The Si-containing impurities could be found by FE-SEM/EDS in the Ni/YSZ, even when using a gold sealing on the Ni/YSZ electrode of the setup (test C); however in smaller quantities than for the Ni/YSZ electrodes of cells testing using the albite glass sealing.

7. The loss in performance for the high current density, high temperature [-2 A/cm^2, 950°C, $p(H_2O) = 0.9$ atm] test D was dominated by a 200% increase in R_s over only 68 h ($\Delta R_p = 21\%/68$ h).

8. FE-SEM of the cell from the high current density, high temperature test D showed significant microstructural changes at the hydrogen electrode/electrolyte interface due to relocation of Ni. A 2–4 μm thick dense layer of Ni and YSZ has formed at the interface caused by relocation of Ni particles. For SOECs aimed at these test conditions different hydrogen electrode materials need to be considered.

Acknowledgments

This work was supported by the EC via the project "Hi2H2" contract no. FP6-503765, by energinet.dk project no. PSO2007-1-7-7124, and by the Danish Programme Committee for Energy and Environment via SERC contract no. 2104-06-0011 and the Danish National Advanced Technology Foundation via contract no. 018-2006-2. Dr. J. R. Bowen is acknowledged for assistance in proofreading of this manuscript.

Risø DTU assisted in meeting the publication costs of this article.

References

1. S. H. Jensen, P. H. Larsen, and M. Mogensen, *Int. J. Hydrogen Energy*, **32**, 3253 (2007).
2. W. Dönitz, R. Schmidberger, E. Steinheil, and R. Streicher, *Int. J. Hydrogen Energy*, **5**, 55 (1980).
3. W. Dönitz, G. Dietrich, E. Erdle, and R. Streicher, *Int. J. Hydrogen Energy*, **13**, 283 (1988).
4. W. Dönitz, E. Erdle, and R. Streicher, in *Electrochemical Hydrogen Technologies. Electrochemical Production and Combustion of Hydrogen*, H. Wendt, Editor, p. 213, Elsevier, London (1990).
5. A. O. Isenberg, *Solid State Ionics*, **3–4**, 431 (1981).
6. N. N. Osada, H. Uchida, and M. Watanabe, *J. Electrochem. Soc.*, **153**, A816 (2006).
7. H. Uchida, N. N. Osada, and M. Watanabe, *Electrochem. Solid-State Lett.*, **7**, A500 (2004).
8. J. E. O'Brien, C. M. Stoots, J. S. Herring, and J. Hartvigsen, *J. Fuel Cell Sci. Technol.*, **3**, 213 (2006).
9. J. S. Herring, J. E. O'Brien, C. M. Stoots, G. L. Hawkes, J. J. Hartvigsen, and M. Shahnam, *Int. J. Hydrogen Energy*, **32**, 440 (2007).
10. O. A. Marina, L. R. Pederson, M. C. Williams, G. W. Coffey, K. D. Meinhardt, C. D. Nguyen, and E. C. Thomsen, *J. Electrochem. Soc.*, **154**, B452 (2007).
11. A. Brisse, J. Schefold, M. Zahid, and A. Aslanides, in *Proceedings of the 2nd World Hydrogen Technologies Convention*, Montecatini Terme, Italy (2007).
12. A. Hauch, S. H. Jensen, M. Mogensen, and S. Ramousse, *J. Electrochem. Soc.*, **153**, A1741 (2006).
13. B. Yidiz and M. S. Kazimi, *Int. J. Hydrogen Energy*, **31**, 77 (2006).
14. M. Ni, M. K. H. Leung, and D. Y. C. Leung, *Chem. Eng. Technol.*, **29**, 636 (2006).
15. W. S. Wang, Y. Y. Huang, S. W. Jung, J. M. Vohs, and R. J. Gorte, *J. Electrochem. Soc.*, **153**, A2066 (2006).
16. S. Elangovan, J. J. Hartvigsen, and L. J. Frost, *Int. J. Appl. Ceram. Technol.*, **4**, 109 (2007).
17. J. Guan, N. Q. Minh, B. Ramamurthi, J. Ruud, J.-K. Hong, P. Riley, and D. Weng, Final Technical Report, DoE Cooperative Agreement DE-FC36-04 GO14351 GE Global Research Center, Niskayuna, NY (2006).
18. C. Mansilla, J. Sigurvinsson, A. Bontemps, A. Marechal, and F. Werkoff, *Energy*, **32**, 423 (2007).
19. A. Hauch, S. H. Jensen, M. Mogensen, and J. B. Bilde-Sørensen, *J. Electrochem. Soc.*, **154**, A619 (2007).
20. P. H. Larsen, C. Bagger, S. Linderoth, M. Mogensen, S. Primdahl, M. J. Jørgensen, P. V. Hendriksen, B. Kindl, N. Bonanos, F. W. Poulsen, et al., in *Solid Oxide Fuel Cells VII*, H. Yokokawa and S. C. Singhal, Editors, PV 2001-16, p. 28, The Electrochemical Society Proceedings Series, Pennington, NJ (2001).
21. A. Hagen, R. Barfod, P. V. Hendriksen, Y. L. Liu, and S. Ramousse, *J. Electrochem. Soc.*, **153**, A1165 (2006).
22. C. Bagger, in *Fuel Cell Seminar*, C. E. Pax, Editor, p. 241, Courtesy Associations, Inc., Washington, DC (1992).
23. M. J. Jorgensen and M. Mogensen, *J. Electrochem. Soc.*, **148**, A433 (2001).
24. R. Barfod, S. Koch, Y.-L. Liu, P. H. Larsen, and P. V. Hendriksen, in *Solid Oxide Fuel Cells VIII*, S. C. Singhal and M. Dokiya, Editors, PV 2003-07, p. 1158, The Electrochemical Society Proceedings Series, Pennington, NJ (2003).
25. M. Mogensen and P. V. Henriksen, *High Temperature Solid Oxide Fuel Cells—Fundamentals, Design and Applications*, p. 261, Elsevier, London (2003).
26. A. Hauch, Ph.D. Thesis, Risø DTU, Technical University of Denmark, Roskilde, Denmark (2007).
27. D. Johnson, *Zview 2.8*, Scribner Associates, Inc., Southern Pines, NC (2003).
28. Y. L. Liu, S. Primdahl, and M. Mogensen, *Solid State Ionics*, **161**, 1 (2003).
29. R. Barfod, A. Hagen, S. Ramousse, P. V. Hendriksen, and M. Mogensen, *6th European Solid Oxide Fuel Cell Forum*, M. Mogensen, Editor, p. 960, European Fuel Cell Forum, Lucerne (2004).
30. R. Barfod, M. Mogensen, T. Klemenso, A. Hagen, Y. L. Liu, and P. V. Hendriksen, *J. Electrochem. Soc.*, **154**, B371 (2007).
31. R. Barfod, M. Mogensen, T. Klemmensoe, A. Hagen, Y. L. Liu, and P. V. Hendriksen, in *Solid Oxide Fuel Cells (SOFC IX)*, S. C. Singhal and J. Mizusaki, Editors, PV 2005-07, p. 524, The Electrochemical Society Proceedings Series, Pennington, NJ (2005).
32. S. H. Jensen, Ph.D Thesis, Risø DTU, Technical University of Denmark, Roskilde, Denmark (2006).
33. A. Hauch, S. D. Ebbesen, S. H. Jensen, and M. Mogensen, *J. Mater. Chem.*, **18**, 2331 (2008).
34. J. B. Bilde-Sørensen, *J. Microsc.*, Submitted.
35. E. J. Opila, D. S. Fox, and N. S. Jacobson, *J. Am. Ceram. Soc.*, **80**, 1009 (1997).
36. N. S. Jacobson, E. J. Opila, D. L. Myers, and E. H. Copland, *J. Chem. Thermodyn.*, **37**, 1130 (2005).
37. J. Hartvigsen, S. Elangovan, J. E. O'Brien, C. M. Stoots, J. S. Herring, and P. Lessing, *6th European Solid Oxide Fuel Cell Forum*, M. Mogensen, Editor, p. 378, European Fuel Cell Forum, Lucerne (2004).
38. S. Primdahl and M. Mogensen, *J. Electrochem. Soc.*, **145**, 2431 (1998).
39. D. Hickey, M. Cassidy, J. McElroy, F. Mitlitsky, and V. Venkataraman, *Solid Oxide Fuel Cells-IX*, p. 285, The Electrochemical Society Inc., Pennington, NJ (2005).
40. T. Matsui, A. Ozaki, R. Kikuchi, and K. Eguchi, in *Solid Oxide Fuel Cells (SOFC IX)*, S. C. Singhal and J. Mizusaki, Editors, PV 2005-07, p. 621, The Electrochemical Society Proceedings Series, Pennington, NJ (2005).
41. A. Momma, T. Kato, Y. Kaga, and S. Nagata, *J. Ceram. Soc. Jpn.*, **105**, 369 (1997).
42. M. Brown, S. Primdahl, and M. Mogensen, *J. Electrochem. Soc.*, **147**, 475 (2000).
43. J. Sehested, J. A. P. Gelten, and S. Helveg, *Appl. Catal., A*, **309**, 237 (2006).
44. A. Hauch, S. H. Jensen, and M. Mogensen, *Solid State Electrochemistry, Proceedings of the 26th Risø International Symposium on Materials Science*, p. 203; S. Linderoth, A. Smith, N. Bonanos, A. Hagen, L. Mikkelsen, K. K. Hansen, D. Lybye, P. V. Hendriksen, F. W. Poulsen, M. Mogensen, et al., Editors, Risø, Roskilde, Denmark (2005).
45. A. E. Hughes and S. P. S. Badwal, *Solid State Ionics*, **46**, 265 (1991).
46. Y. L. Liu, K. Thydén, Q. Xing, and E. Johnson, *Solid State Electrochemistry, Proceedings of the 26th Risø International Symposium on Materials Science: Solid State Electrochemistry*, Risø, Roskilde, Denmark, p. 273; S. Linderoth, A. Smith, N. Bonanos, A. Hagen, L. Mikkelsen, K. K. Hansen, D. Lybye, P. V. Hendriksen, F. W. Poulsen, M. Mogensen, et al., Editors, Risø, Roskilde, Denmark (2005).
47. Y.-L. Liu and C. Jiao, *Solid State Ionics*, **176**, 435 (2005).
48. A. Hauch, J. Bowen, L. Theil-Kuhn, and M. Mogensen, *Electrochem. Solid-State Lett.*, **11**, B38 (2007).